Unusual Intramolecular Motion of ReH$_9^{2-}$ in K$_2$ReH$_9$ Crystal: Circle Dance and Three-Arm Turnstile Mechanisms Revealed by Computational Studies

Yunwen Tao,* Xianlong Wang,* Wenli Zou, Geng-Geng Luo, and Elfi Kraka*

Read Online

ACCESS | Metrics & More | Article Recommendations | SI Supporting Information

ABSTRACT: The nonahydridorhenate dianion ReH$_9^{2-}$ is a unique rhenium polyhydride complex due to its remarkably high coordination number; however, its detailed polytopal rearrangement process in either solution or crystal is so far unclear. In this work, our quantum chemical calculations have identified two previously unreported fluxional mechanisms for the ReH$_9^{2-}$ dianion in the K$_2$ReH$_9$ crystal: three-arm turnstile rotation and circle dance mechanism. These two polytopal rearrangements in the crystal offer an alternative interpretation to the pulse and wide-line NMR spectra (Farrar et al. *J. Chem. Phys.* **1969**, 51, 3595). The previously postulated hindered rotation of the whole ReH$_9^{2-}$ dianion in K$_2$ReH$_9$ (White et al. *J. Chem. Soc., Faraday Trans. 2* **1972**, 68, 1414) turns out to be a combination of the above-mentioned two elementary fluxional processes. In addition, our calculations have confirmed the Muetterties' $D_{3h} \rightleftharpoons C_{4v}$ rearrangement as the intramolecular motion for the ReH$_9^{2-}$ dianion in solution.

ReH$_9^{2-}$ in K$_2$ReH$_9$ crystal
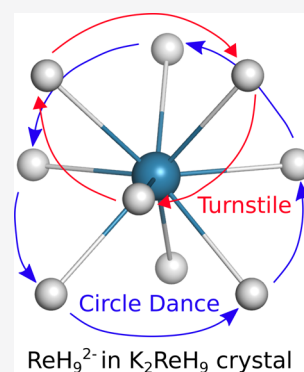
INTRODUCTION

The stereochemical nonrigidity of coordination compounds especially in solids represents a very attractive but often overlooked research field in inorganic chemistry. The term "polytopal rearrangement" in coordination compounds describes a dynamical process that changes the ligand position in the coordination polyhedra.[1−4] One prominent example of this type of fluxionality is the Berry pseudorotation[5−7] in tetra-/pentavalent compounds, while it includes but is not limited to the lever mechanism in SF$_4$,[8] the Muetterties' mechanisms in pentacoordinate compounds,[2,9] the chimeric pseudorotation in IF$_5$,[10] Bailar and Ray-Dutt twists in hexacoordinate compounds,[11,12] and the Bartell pseudorotation in IF$_7$.[13] Besides serving as an important type of fluxionality in coordination compounds, polytopal rearrangements have been utilized in designing self-healing polymers[14] and tweaking the reactivity of various homogeneous catalysts.[15−20] NMR spectroscopy measuring parameters like chemical shift, relaxation times, second moment, line shape, etc. have been often employed to characterize the polytopal rearrangement processes because NMR covers a wide time scale ranging from 10^2 to 10^{-10} s for any fluxional process.[21−23] The atomistic mechanism of some polytopal rearrangement processes has be deduced from the continuous shape measure (CShM) method,[24,25] which collects from databases all intermediate structures on a conceptual path connecting two reference polyhedra. However, a more general applicable option is to employ quantum chemical calculations to validate or even predict the polytopal rearrangement processes by tracing out the detailed pathway or trajectory of the atomic nuclei.[10,26−29]

As part of our continuing investigation of the polytopal rearrangements for coordination complexes with a coordination number larger than seven,[30,31] we chose the nonahydridorhenate dianion ReH$_9^{2-}$ as the subject to be studied in this work because it is a paradigmatic nonacoordinate compound while its detailed polytopal rearrangement mechanism is so far unknown.

The ReH$_9^{2-}$ dianion as the first example of a nine-coordinate homoleptic metal hydride adopts a tricapped trigonal prism (TTP) geometry.[32] Other nonacoordinate complexes generally can also adopt a monocapped square antiprism (MSA), capped cube (CCU), tridiminished icosahedron (TDIC), hula hoop (HH), muffin (MFF), or pentagonal interpenetrating tetrahedral polyhedron (PITP) geometry.[33,34] The nine hydrogen atoms in ReH$_9^{2-}$ can be divided into two groups including (1) six prism hydrogens located at the prism vertices and (2) three equatorial cap hydrogens sticking out of the prism side faces. The molecular structure of ReH$_9^{2-}$ dianion was first resolved in the K$_2$ReH$_9$ crystal by Ginsberg and co-workers using single crystal X-ray and neutron diffraction in 1964.[35,36] Bronger and co-workers redetermined the K$_2$ReH$_9$ crystal structure with neutron diffraction analysis in 1999 and obtained the structure
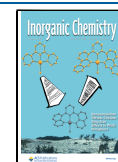
with improved accuracy.[37] Over the past six decades, a series of experimental studies have been carried out to delineate the vibrational properties of ReH_9^{2-} in crystals,[38−42] and the high-pressure phases of some ionic ReH_9^{2-} salts (e.g., $BaReH_9$) were pursued as potential superconductors.[43,44] Numerous theoretical studies were conducted on ReH_9^{2-} including its structure, vibrational spectra, chemical bonding properties, and high-pressure induced structural changes of related crystals.[42,43,45−47]

However, there are only scattered reports in the literature on the fluxionality of ReH_9^{2-} or other nonacoordinate homoleptic metal hydride complexes (e.g., TcH_9^{2-}). In their seminal work published in 1964, Ginsberg and co-workers showed that the ^1H NMR spectrum of K_2ReH_9 solution has only one single line demonstrating the fluxionality of the hydride ligands in the ReH_9^{2-} dianion for the first time.[36] A potential polytopal rearrangement pathway, which exchanges the prism and cap hydrogens (i.e., pseudorotation[1]), was attributed to a low-frequency vibration of the dianion. In 1969, Farrar and co-workers studied the fluxionality of ReH_9^{2-} in the K_2ReH_9 solid with pulsed and wide-line NMR.[48] They obtained the activation energies for the internal reorientation of the ReH_9^{2-} dianions at two distinct Wyckoff positions from the spin−lattice relaxation times (T_1). However, the actual dynamics of this reorientation remained elusive. In 1972, White and Wright assumed that the ReH_9^{2-} dianions would undergo hindered rotation (i.e., libration) in the K_2ReH_9 solid and then used incoherent neutron scattering (INS) spectroscopy to measure the frequencies of the libration modes of ReH_9^{2-} around different axes in the crystal environment.[40] The estimated barriers of the hindered rotation derived from the INS data approximately match the barriers from NMR study in 1969, but the INS result excluded the possibility of isotropic rotation of ReH_9^{2-} dianions in K_2ReH_9. Noteworthy is a very recent work by Takagi and co-workers who computationally studied the collective rotation of OsH_9^{2-} and ReH_9^{2-} dianions in Cs_3OsH_9 and Cs_3ReH_{10} crystals, respectively.[49] An interesting pseudorotation process for the OsH_8^{2-} unit was discovered with a low energy barrier (∼0.2 kcal/mol) but the authors did not further delve into the intramolecular dynamics of ReH_9^{2-}.

The above-mentioned literature has also brought to our attention the polytopal rearrangement in crystalline structures. While there have been numerous reports on the internal rotation of functional groups as molecular rotors in crystals[50−53] (one of us wrote a dedicated book on this topic[54]), the polytopal rearrangement of coordination compounds is rarely observed in solids because the movement of ligands in such closely packed environments is rather difficult and the ligands have to be highly mobile.[22] Reports on the polytopal rearrangement in solids include (1) the solid of Tungsten complex $W(PMe_3)_3H_6$,[55] (2) TaF_7^{-2} anion in the $(NH_4)_2TaF_7$ solid,[56] and (3) the OsH_8^{-2} anion in Cs_3OsH_8.[49] To our best knowledge, polytopal rearrangement processes in solids are only possible for compounds whose coordination number is above six with small displacements of the ligating atoms because the polytopal rearrangement with large-amplitude motion for lower coordinated counterparts in solids is energetically prohibited.

In this context, we aim to understand the polytopal rearrangement of the ReH_9^{2-} anion in solution as the starting point. Then, for the ReH_9^{2-} anion in solids, we are not only interested to find possible intramolecular motions (i.e., polytopal rearrangement) besides the reported hindered rotation[40] but also to understand the relationship between the intramolecular motions and hindered rotation.

■ COMPUTATIONAL DETAILS

The *ab initio* molecular dynamics (AIMD) simulation of the ReH_9^{2-} dianion in gas phase was conducted at the M06-L/def2-SVP level[57−59] using the ORCA 4.1.1 program.[60] Five temperatures (100, 200, ..., and 500 K) were selected to run the simulation for 25 ps each. The Berendsen thermostat[61] was employed to control the simulation temperature and the simulation time step was set to 0.5 fs.

Geometry optimization for transition state (TS) structure for the $D_{3h} \rightleftharpoons C_{4v}$ rearrangement process of the ReH_9^{2-} dianion was conducted at the M06-L/def2-SVP level[57−59] using the Gaussian 16 program[62] based on a selected AIMD snapshot structure as the initial guess. The local-minimum structure of ReH_9^{2-} dianion was optimized at the same level of theory. The single-point energies of the optimized structures were calculated at the DLPNO−CCSD(T)/ma-def2-TZVP level[58,59,63] with "TightPNO" settings using the ORCA program.[60]

The AIMD of the K_2ReH_9 crystal was carried out on a primitive cell model using the VASP 5.4.4 package.[64−67] The Perdew−Burke−Ernzerhof (PBE)[68,69] density functional was employed with the projector-augmented wave (PAW) potential[70,71] and the kinetic energy cutoff was set by default according to the "medium" precision settings. The convergence criterion of wave function optimization was set to 10^{-4} eV to speed up the calculation. The canonical (NVT) ensemble simulation was conducted at 300 K for 5 ps with the time step of 0.5 fs, and the simulation was run five times to sample sufficient configurations. The Nose-Hoover thermostat was used to control the temperature, and the unit cell was fixed during the simulation.

The primitive cell structure of K_2ReH_9 was optimized using the revPBE[72] density functional with the VASP package.[64−67] The kinetic energy cutoff of basis set was set to 359 eV. The wave function was considered converged when the energy difference was smaller than 10^{-7} eV in each iteration step. The cell optimization was terminated while the atomic forces were smaller than 10^{-4} eV/Å.

The Henkelman's climbing image nudged elastic band (ci-NEB) method[73,74] implemented in a modified version of the VASP program[64−67] was employed to search for the transition state structures and the minimum energy pathways for the two new fluxional processes in K_2ReH_9. The optimized primitive cell structure of K_2ReH_9 was used as the initial and final end points for ci-NEB calculations. The two end point structures differ in the labels (i.e., ordering) of three or five hydrogens (depending on the type of the intramolecular rearrangement) in ReH_9^{2-} dianion at site *a* or *d*. To be more specific, the labels for the involved hydrogens were shifted to their neighboring hydrogens in a circular fashion. Between each pair of initial and final end points, six intermediate bead guess structures were generated via linear interpolation leading to in total six images for one ci-NEB calculation setup. During the ci-NEB calculations, the fast inertial relaxation engine (FIRE) algorithm was first used for initial optimization and then the limited-memory Broyden-Fletcher-Goldfarb-Shanno (LBFGS) algorithm was employed to refine the ci-NEB images.[75] All ci-NEB calculations were completed when the tangential forces converged to 0.001 eV/Å.

The vibrational frequencies of the saddle point and local minimum structures of K_2ReH_9 crystal were calculated on a primitive cell model based on the density-functional perturbation theory (DFPT).[76] The thermal correction to the Helmholtz free energy arising from lattice vibrations was calculated with the help of the Phonopy package.[77]

All calculations were conducted using the computational nodes equipped with dual Intel Xeon E5−2695 v4 CPUs (36 CPU cores) in the ManeFrame II computing facility at SMU.

■ RESULTS AND DISCUSSION

Polytopal Rearrangement of ReH_9^{2-} in Solution. To study the fluxionality of the ReH_9^{2-} dianion in solution, we carried out the *ab initio* molecular dynamics (AIMD) simulations of the isolated ReH_9^{2-} dianion. The choice of the gas-phase model over explicit solvation model in AIMD calculation is justified because we are interested in the intramolecular motions of the dianion while the possible intermolecular mechanism (e.g., hydrogen exchange[78]) between ReH_9^{2-} and water is temporarily beyond the scope of this study.

After projecting out the overall translations and rotations of ReH_9^{2-} during the AIMD simulation by aligning to the first MD snapshot, we carefully examined the atomistic motions of the dianion in each trajectory. We found that the structural variation in ReH_9^{2-} during the AIMD simulation is in line with the $D_{3h} \rightleftharpoons C_{4v}$ rearrangement mechanism (see Figure 1)
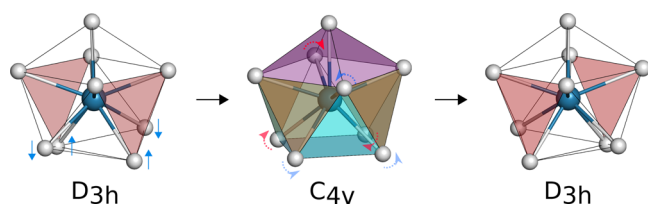

Figure 1. Polytopal rearrangement process of isolated ReH_9^{2-} dianion. This fluxional process starts from the faced-tricapped trigonal prism structure in D_{3h} symmetry (left), passes the monocapped square antiprism structure in C_{4v} symmetry as the transition state (middle), and ends with another faced-tricapped trigonal prism structure (right) equivalent to the starting structure. In D_{3h} structures, prism hydrogens constitute two red triangles while the remaining are cap hydrogens.

proposed by Guggenberger and Muetterties in 1976.[79] We successfully located the transition state (TS) for this rearrangement process. Therefore, this $D_{3h} \rightleftharpoons C_{4v}$ rearrangement process featuring the monocapped square antiprism (MSA) structure as the TS is confirmed for ReH_9^{2-} (corresponding Cartesian coordinates are given in the Supporting Information). As the electronic energy barrier for this $D_{3h} \rightleftharpoons C_{4v}$ rearrangement at the DFT level is as low as 0.3 kcal/mol, we re-evaluated the electronic barrier height at the DLPNO−CCSD(T) level[63] as 0.27 kcal/mol. Besides, our examination of the AIMD trajectories demonstrates that the seemingly complicated scrambling behavior of hydrogens in ReH_9^{2-} actually consists of a series of successive $D_{3h} \rightleftharpoons C_{4v}$ rearrangements (see Supporting Information Table S1 and Figures S1−S2 for more details) while no other type of intramolecular rearrangement was observed even at elevated simulation temperature up to 500 K. This suggests that the $D_{3h} \rightleftharpoons C_{4v}$ mechanism is the only feasible polytopal rearrangement process for ReH_9^{2-} in solution and such assertion is made based on two factors. First, the spatial layout of the ligands in

the nonacoordinate ReH_9^{2-} is highly congested; therefore, an individual hydrogen can not move freely; it has to move together with other hydrogens. Second, the energy barrier for the $D_{3h} \rightleftharpoons C_{4v}$ rearrangement is so low that any other possible intramolecular rearrangement pathway would be bypassed.

Polytopal Rearrangement of ReH_9^{2-} in K_2ReH_9 Crystal. The crystalline structure of K_2ReH_9 ($P\bar{6}2m$ space group) has two crystallographically distinct sites for the ReH_9^{2-} dianion including site *a* and site *d* with their ratio of 1:2.[35−37] Both sites have the ReH_9^{2-} dianion in the center surrounded by nine potassium cations (see Figure 2), and these two sites have minor structural differences leading to D_{3h} and C_{3h} symmetries for sites *a* and *d*, respectively.
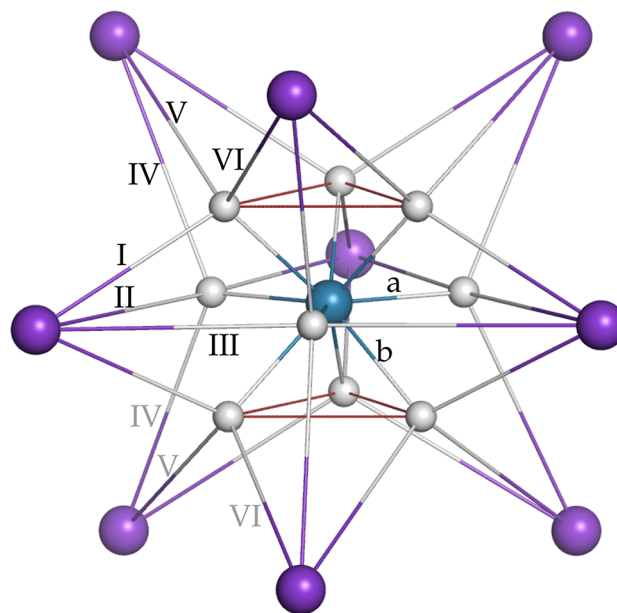

Figure 2. Structure of ReH_9^{2-} dianion encapsulated by nine vicinal K^+ cations in the K_2ReH_9 crystal. Two parallel trigonal faces within the prism structure are outlined in red color. The cap and prism Re−H bonds are labeled with a and b, respectively. Different K···H interactions are labeled with Roman numerals I−VI.

To examine the fluxionality of the ReH_9^{2-} dianion within the K_2ReH_9 crystal, we used the primitive cell structure of K_2ReH_9 containing both dianion sites and performed AIMD simulations on it. As the overall translations and rotations of the simulation cell are intrinsically eliminated, the analysis of the motions of ReH_9^{2-} in K_2ReH_9 solid during AIMD simulations is straightforward. To search for the reported hindered rotation[40] of the whole ReH_9^{2-} dianion and any possible intramolecular rearrangement, we carefully inspected each dianion site by coloring the nine hydrogens in ReH_9^{2-} distinctively and then superimposing all snapshots of an AIMD trajectory for ReH_9^{2-} dianions. In this way, one can clearly see the path each hydrogen atom traverses during AIMD simulations from its starting location. From our analysis on the AIMD trajectories within limited time scale, we observed no occurrence of the rotation of the whole ReH_9^{2-} dianion. For the majority of the simulation time, the ReH_9^{2-} dianions only fluctuated in the vicinity of their equilibrium positions as revealed by nine well-separated clusters resulting from the superposition of AIMD snapshots for the hydride ligands (see Supporting Information Figure S3). However, we

identified from AIMD trajectories two distinct types of intramolecular motions that can interchange the positions of hydride ligands in ReH_9^{2-} for both site *a* and *d* in K_2ReH_9.

The first type of isomerization is a 3-fold rotation involving two neighboring prism hydrogens and one vicinal cap hydrogen as a triad (see Figure 3 and Supporting Information
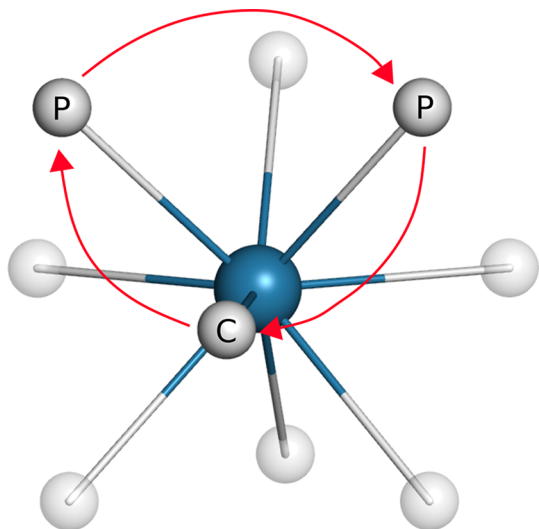

Figure 3. Schematic representation of the turnstile rotation mechanism in ReH_9^{2-} dianion within the K_2ReH_9 crystal. Two prism (P) and one cap (C) hydrogens involved in this intramolecular motion are highlighted. The orientation of the ReH_9^{2-} dianion in this figure is consistent with that in Figure 2. The calculated energy barriers $\Delta E^{\ddagger}$ with revPBE density functional at site *a* and *d* are 2.89 and 6.99 kcal/mol, respectively.

Figure S4). Such rearrangement for hydride ligands in transition metal complexes has been frequently reported in the literature and named three-arm turnstile rotation.[31,80] Because of the symmetry of ReH_9^{2-} in K_2ReH_9, this turnstile rotation can occur for any one out of six triads of this type in either direction. An interesting and counterintuitive aspect is that this turnstile rotation was not observed for three adjacent prism hydrogens around the C_3 axis but only for a tilted triad of hydrogens in our AIMD calculations although the former triad of three prism hydrogens seems more likely to undergo turnstile rotation. This could be a result of a reduced barrier height for the tilted set of hydrogens, and we need to note that no turnstile rotation around the C_3 axis for three adjacent prism hydrogens was observed in the AIMD of ReH_9^{2-} in gas phase either.

The second type of isomerization is a 5-fold cyclic rotation involving three prism hydrogens and two cap hydrogens as a quintet and these five hydrogens lie almost in a plane (see Figure 4 and Supporting Information Figures S5 and S9). After each 5-fold rotation step (ca. 72°), the resulting ReH_9^{2-} structure is indistinguishable from the starting structure because the concerned five hydride ligands have moved to their optimal neighboring locations. Similar to the above-mentioned three-arm turnstile rotation, this 5-fold rotation also has two equivalent rotational directions due to symmetry and it occurs for six different sets of quintet for ReH_9^{2-} in K_2ReH_9.

Apart from the two above-mentioned intramolecular rotations of hydrogens, we did not observe any other type of intramolecular motions in our AIMD trajectories. However, it is still an open question whether the above two intramolecular
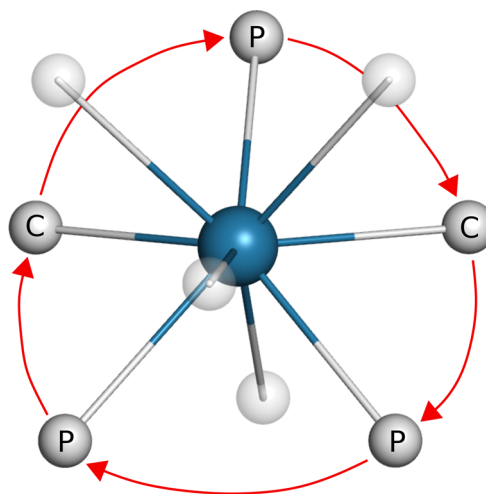

Figure 4. Schematic representation of the circle dance mechanism in ReH_9^{2-} dianion within the K_2ReH_9 crystal. Three prism (P) and two cap (C) hydrogens involved in this intramolecular motion are highlighted. The orientation of the ReH_9^{2-} dianion in this figure is consistent with that in Figure 2. The calculated energy barriers $\Delta E^{\ddagger}$ with revPBE density functional at site *a* and *d* are 4.68 and 5.47 kcal/mol, respectively.

isomerizations are elementary fluxional processes or either isomerization is a result of several basic fluxional steps. Therefore, we need to validate these two isomerization mechanisms by finding their transition states and calculate corresponding barrier heights. In addition, we may check whether the calculated energy barriers could match the experimentally measured values with NMR[48] and INS[40] so that the underlying fluxional processes can be revealed.

By comparing the AIMD simulation results for the ReH_9^{2-} dianion in gas phase and in K_2ReH_9 crystal, we realized that the aforementioned two isomerization processes in the K_2ReH_9 crystal are susceptible to the potassium cations surrounding the ReH_9^{2-} dianion.[47] Therefore, the calculated energy barriers of fluxional processes in K_2ReH_9 are coupled to the prediction of interatomic distances and lattice parameters by DFT. To select a density functional that can best reproduce the experimentally resolved crystal structure of K_2ReH_9, we tested four generalized gradient approximation (GGA) density functionals including PBE,[68,69] PW91,[81,82] revPBE,[72] and PBEsol[83] as well as the meta-GGA density functional TPSS[84] to relax the atomic positions and cell parameters of K_2ReH_9 simultaneously. The density functional revPBE[72] outperforms the other selected density functionals in predicting the lattice parameters and is more cost-efficient than meta-GGA density functionals (see Supporting Information Table S2). Table 1 lists the calculated lattice parameters and key bond lengths (labeled in Figure 2) in K_2ReH_9. The data show that the percentage error between the calculated and experimentally measured values[37] is less than 2%, which demonstrates the high reliability of the revPBE density functional for describing the K_2ReH_9 system. In addition, our calculation perfectly retained the D_{3h} and C_{3h} symmetries for sites *a* and *d*, respectively.

With the optimized primitive cell structure of K_2ReH_9 at the revPBE/PAW level, further calculations to unravel the atomistic mechanisms of the two possible intramolecular rearrangements as shown in Figures 3 and 4 were conducted at the same level of theory. We successfully located the saddle

Table 1. Experimental and Computed Cell Parameters and Key Bond Lengths in K_2ReH_9 Crystal Structure[a,b]

Cell Parameter				
$a_1 = a_2$	9.599 (9.662, 0.7)	$\alpha = \beta$	90° (90°, 0.0)	
a_3	5.549 (5.647, 1.8)	γ	120° (120°, 0.0)	
Bond Length		Site d $[C_{3h}]$	Site a $[D_{3h}]$	
Re−H	a	1.673 (1.687, 0.8)	1.679 (1.689, 0.6)	
	b	1.703 (1.717, 0.8)	1.690 (1.711, 1.2)	
K···H	I	2.689 (2.715, 1.0)	2.956 (2.979, 0.8)	
	II	3.090 (3.130, 1.3)	3.441 (3.429, − 0.3)	
	III	3.129 (3.130, 0.0)	3.441 (3.429, − 0.3)	
	IV	3.034 (3.086, 1.7)	2.899 (2.948, 1.7)	
	V	2.909 (2.956, 1.6)	2.720 (2.731, 0.4)	
	VI	3.017 (3.053, 1.2)	2.720 (2.731, 0.4)	

[a]Cell parameters a_1-a_3 and bond lengths are given in Angstrom (Å). The definition of bond is shown in Figure 2. [b]Computed structural parameter value at revPBE/PAW level is given in parentheses after the experimental value[37] followed by the percentage error.

point structures from the climbing image nudged elastic band (ci-NEB)[73,74] calculations on K_2ReH_9 (corresponding Cartesian coordinates are given in the Supporting Information) and the electronic energy barriers at site a for three-arm turnstile and 5-fold rotation mechanism are 2.89 and 4.68 kcal/mol, while the barriers for these two mechanisms at site d are 6.99 and 5.47 kcal/mol, respectively (see Table 2). In addition, we

Table 2. Calculated and Experimentally Measured Energy Barriers (in kcal/mol) of Fluxional Processes in K_2ReH_9[a]

		turnstile	circle dance	NMR[b]	INS[c]
site a	$\Delta E^{\ddagger}$	2.89	4.68	2.4(3.1)	4.1
	$\Delta A^{\ddagger}$	3.66	5.49		
site d	$\Delta E^{\ddagger}$	6.99	5.47	6.0(6.9)	8.8
	$\Delta A^{\ddagger}$	7.78	6.58		

[a]$\Delta E^{\ddagger}$ and $\Delta A^{\ddagger}$ represent the calculated electronic energy barrier at 0 K and the Helmholtz free energy barrier at 165 K, respectively. [b]Experimentally measured energy barrier is derived from spin−lattice relaxation time (T_1).[48] Values in parentheses are the energy barriers added with zero-point energy of degenerate vibration.[40] [c]Experimentally measured energy barrier is obtained from librations around $2C_2$ axes characterized by the incoherent neutron scattering (INS).[40]

conducted vibrational frequency calculations on the saddle point structures and obtained only one imaginary frequency while the remaining $3N − 4$ vibrational frequencies are all real (N is the number of atoms in the primitive cell model of K_2ReH_9).

These results confirm that the three-arm turnstile rotation and the 5-fold rotation are two elementary polytopal rearrangement mechanisms of the ReH_9^{-2} dianion in K_2ReH_9. As the motion of five hydride ligands in the 5-fold rotation mechanism bears similarities to the circle dance in reminiscence of the famous painting by Henri Matisse (see Figure 5), we name this fluxional mechanism "circle dance" in the following.

We calculated the thermal correction to the Helmholtz free energy arising from vibrations on the saddle point and equilibrium structures and then obtained the Helmholtz free energy barriers at 165 K as listed in Table 2 so that these values can be compared with experimentally measured values. The reason why we chose this temperature is because it splits the

Figure 5. Matisse, Henri. *Dance (II)*. 1910, Hermitage Museum, Saint Petersburg, Russia. *WikiArt.org*, https://en.wikipedia.org/wiki/File:Matissedance.jpg (accessed on 11-19-2021).

T_1 profile measured by Farrar et al.[48] into two distinct regions, although other temperatures (e.g., 90 K[40]) are also a reasonable choice. We found that the thermal correction to four energy barriers ranges from +0.8 to +1.1 kcal/mol, and the barrier of the three-arm turnstile mechanism at site a is lower than that of the 5-fold rotation by 1.8 kcal/mol, while the barrier of the 5-fold rotation mechanism at site d is lower than that of the turnstile rotation by 1.2−1.5 kcal/mol.

We notice from Table 2 that the calculated energy barriers of both fluxional mechanisms in K_2ReH_9 at site a are lower than those at site d by 1−2 kcal/mol. Such difference was attributed to the spatial arrangement of surrounding dianions at these two sites by Farrar and co-workers.[48] However, we believe the direct reason for such barrier difference is on the K···H electrostatic interactions. Calculations by Schaefer and co-workers demonstrated in a model K_2ReH_9 molecule that there exists electrostatic attraction between the potassium cations and the hydride ligands with partial negative charges.[47] Therefore, such electrastatic attraction could stabilize the ReH_9^{2-} dianions in K_2ReH_9 crystal. As shown in Figure 2 and Table 1, the major difference in the K···H interaction between two sites in K_2ReH_9 is from interactions II and III. For site a, K···H interactions II and III have the interatomic distances up to 3.4 Å while the longest electrostatic attraction at site d is interaction III (3.1 Å). Longer distance of electrostatic attraction may lead to marginally weaker stabilization effect on the ReH_9^{2-} dianion at site a, which renders more structural flexibility and lowers the barriers of the two fluxional mechanisms. Given the fact that the potassium cations give rise to the three-arm turnstile and circle dance mechanisms for the ReH_9^{2-} dianion in K_2ReH_9 when comparing the AIMD results of this dianion in gas phase and in crystal structure, the K···H electrostatic attraction plays a dual role in supporting and suppressing these two fluxional mechanisms.

Before a direct comparison between our calculated energy barriers of two fluxional mechanisms and the experimentally measured values, the inconsistency between our calculated intramolecular motions of ReH_9^{2-} and the reported libration of the whole ReH_9^{2-} dianion in K_2ReH_9 needs to be resolved.

In the seminal work of Farrar and co-workers,[48] they measured the ^1H spin−lattice relaxation time (T_1) of K_2ReH_9 at 19.0 MHz and obtained the profile of T_1 as a function of temperature (T). Two local minima at T = 143 K and T = 250 K were interpreted as two different ReH_9^{-2} dianions reorienting

at different temperatures. On the basis of the different contributions to the total relaxation rate R_1[85,86] from dianion sites a and d, two minima of T_1 were unambiguously assigned to these two sites due to the shorter T_1 expected for site d than for site a. By calculating the correlation time (τ_c) for two sites from the T_1 profile, the Arrhenius' equation of T_1 was employed to calculate the activation energies of reorientation in ReH_9^{-2} at site a and d as 2.4 and 6.0 kcal/mol, respectively. Furthermore, they measured the second moment (M_2) of the protons at different temperatures and calculated both the intraionic and interionic contributions to M_2 based on the resolved K_2ReH_9 crystal structure. The measured M_2 for the rigid structure at low temperature is about 35 G^2 and it drops to two-thirds when the temperature increases to 90−125 K. As the temperature continues to rise, M_2 drops to 1 G^2, which is basically the interionic contribution without any intraionic contributions. This result was interpreted that in the T = 90−125 K region the reorientation could occur only for site a while the site d is rigid and in the room temperature both sites could undergo reorientation. They assumed that the reorientation would be the overall rotation of the ReH_9^{-2} dianion and such rotation could be isotropic at room temperature because of the fact that the rotation of spins results in the averaging of the local magnetic fields and thus reduces the M_2 value.[87,88] However, their assumption could be problematic because the possibility of intramolecular rotation of hydrogens within ReH_9^{-2} was overlooked.

If we consider the two fluxional mechanisms discovered in this work for K_2ReH_9, both the three-arm turnstile rotation and the circle dance mechanism are rotations of a subset of nine hydrogens in each ReH_9^{-2} dianion. Therefore, both mechanisms at either site can reduce M_2 as temperature increase. We also need to note that for each ReH_9^{-2} dianion site, either mechanism (involving both prism and cap hydrogens) can occur at six different locations with the same probability and this could also lead to the complete elimination of the intraionic contribution to M_2 as revealed by NMR. In this way, we provide an alternative interpretation of the measured M_2 profile.

For either dianion site in K_2ReH_9, two fluxional mechanisms have slightly different energy barriers and the one with relatively lower barrier can be first activated at low temperature to effect the NMR spectra before the one with higher barrier. At a higher temperature, both fluxional mechanisms at either site can effect the NMR spectra. Thus, it is justified to compare the fluxional mechanism with lower calculated energy barrier at either site with NMR measurement in terms of barrier height. As shown in Table 2, our calculated values of the lower electronic energy barriers at two sites (2.89 and 5.47 kcal/mol for a and d, respectively) are very close to the NMR energy barriers (2.4 and 6.0 kcal/mol). While the calculated average free energy barriers (3.66 and 6.58 kcal/mol) are slightly higher than their electronic counterparts, the difference between two sites (2.9 kcal/mol) is still close to the difference in NMR barriers (3.6 kcal/mol). Therefore, we conclude that our calculated energy barriers match well with the barriers measured by NMR and the two newly discovered fluxional mechanisms in this work are feasible motions in K_2ReH_9.

In the work by White and Wright[40] following the above-mentioned NMR studies on K_2ReH_9, they mistakenly adopted the idea that the ReH_9^{2-} dianion could have external rotations within the lattice structure and employed the incoherent neutron scattering (INS) spectroscopy to characterize the

libration motion of ReH_9^{2-} dianions in the crystal structures. They used the harmonic oscillator formula to derive the barriers for the external rotations of ReH_9^{2-} around its $2C_2$ axes and found these values are close to the above-mentioned NMR barriers. Thus they concluded that the libration of ReH_9^{2-} about the $2C_2$ axes was confirmed, whereas the libration about the C_3 axis was not.

An important question arises: why do the barriers derived from INS studies match with those from NMR experiments even though our calculated fluxional mechanisms have excluded the possibility of external rotation being an elementary fluxional process in ReH_9^{2-}? It is important to note that the three-arm turnstile and the circle dance mechanisms coexist in K_2ReH_9 and they can be superimposed in the way that eight hydrogen atoms participating in these two mechanisms lead to the overall rotation of ReH_9^{2-} structure about an axis, which is approximately parallel to the remaining Re−H bond (see Figure 6 and Supporting Information Figure
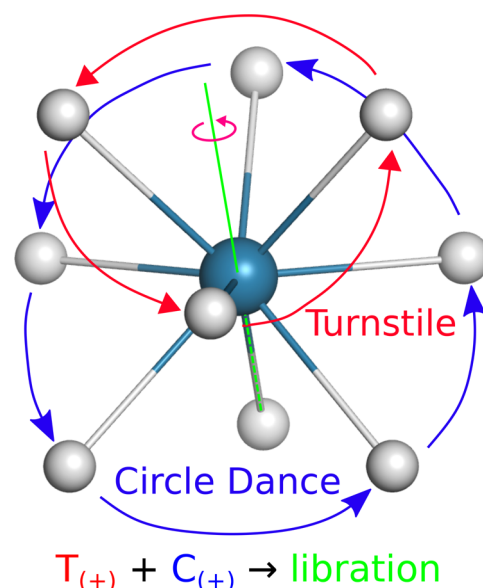

Figure 6. Schematic representation of the overall libration motion of hydrogens in K_2ReH_9 around the axis (colored in green) as a result of the combination of the three-arm turnstile rotation (color in red) and the circle dance mechanism (color in blue) in the same counter-clockwise (+) direction. The orientation of the ReH_9^{2-} dianion in this figure is consistent with that in Figure 2.

S10). In addition, these two intramolecular rotation mechanisms need to be in the same direction. To achieve such an overall rotation, two fluxional mechanisms cannot occur simultaneously but in a consecutive manner. Therefore, only the rate limiting step with higher energy barrier can be compared with the barriers derived from the INS experiment. As shown in Table 2, the agreement between our values (5.49 and 7.78 kcal/mol) and the INS barriers (4.1 and 8.8 kcal/mol) is satisfactory, although the INS barriers are slightly higher, which is caused by the rudimentary choice of the $2C_2$ axes.

The above analysis has now resolved the inconsistency between the two fluxional mechanisms revealed by our calculations and the hindered rotation of ReH_9^{2-} within K_2ReH_9 reported in the literature.[40,48] In this aspect, we see that the advanced NMR and INS spectroscopic techniques are able to provide accurate activation barrier data of fluxional

processes, but they can offer quite limited information about the detailed atomistic motions and erroneous interpretation of spectra is sometimes inevitable. Quantum chemical simulation of the fluxional processes is an important complement to the spectroscopic experiments. It is also worth noting that our calculations in this work did not include the quantum mechanical tunneling effect of the H atoms, which sustains the fluxional motions of ReH_9^{2-} in the crystal at low temperature.

CONCLUSIONS

In conclusion, our work has confirmed Muetterties' $D_{3h} \rightleftharpoons C_{4v}$ interconversion[79] as the polytopal rearrangement mechanism of ReH_9^{2-} dianion in solution based on the AIMD calculation of this dianion in gas phase. In addition, we discovered for the ReH_9^{2-} dianion in K_2ReH_9 the three-arm turnstile rotation and the circle dance mechanism as two polytopal rearrangements and also as two internal rotations in crystalline structures by applying the AIMD and ci-NEB[73,74] techniques. These two fluxional mechanisms of ReH_9^{2-} are faciliated by the K···H electrostatic attraction, which directly impacts their energy barriers. On the basis of our calculations, we provide in this work an alternative interpretation of the previously reported ^1H second moment spectra of K_2ReH_9, and the satisfactory agreement between our calculated energy barriers of these two mechanisms and the barriers derived from ^1H spin−lattice relaxation time (T_1)[48] clearly identifies these two mechanisms as elementary fluxional processes of ReH_9^{2-} in K_2ReH_9. Given the similar energy barriers of these two mechanisms at either site a or d in K_2ReH_9, the coexistence of these two intramolecular rotations can lead to the external rotation of ReH_9^{2-} in the crystal. This explains why the previously measured energy barriers from the libration of ReH_9^{2-} examined by the incoherent neutron scattering (INS) spectroscopy[40] could approximately match the NMR barriers and our calculated values. We believe that the two newly discovered polytopal rearrangements in K_2ReH_9 may exist not only in the crystals containing the ReH_9^{2-} dianion (e.g., K_2ReH_9 and $BaReH_9$) but also in the crystals having other nonacoordinate homoleptic metal hydrides (e.g., TcH_9^{2-}).[32,89] We hope this work could spur interest in exploring the fluxionality of compounds with high coordination number among both experimental and theoretical chemists.

ASSOCIATED CONTENT

ⓈI Supporting Information

The Supporting Information is available free of charge at https://pubs.acs.org/doi/10.1021/acs.inorgchem.1c03118.

> Example AIMD simulation trajectory for ReH_9^{2-} dianion in gas phase; multiframe animation of three-arm turnstile rotation of ReH_9^{2-} dianion in K_2ReH_9; multiframe animation of circle dance mechanism of ReH_9^{2-} dianion in K_2ReH_9; computational details and additional computational results (ZIP)

AUTHOR INFORMATION

Corresponding Authors

    Yunwen Tao − *Department of Chemistry, Southern Methodist University, Dallas, Texas 75275-0314, United States*; Email: ywtao.smu@gmail.com

    Xianlong Wang − *Department of Bioinformatics, School of Medical Technology and Engineering, Key Laboratory of Medical Bioinformatics, Key Laboratory of Ministry of Education for Gastrointestinal Cancer, Fujian Medical University, Fuzhou 350122, P. R. China; School and Hospital of Stomatology, Fujian Medical University, Fuzhou 350002, P. R. China*; Email: wang.xianlong@139.com

    Elfi Kraka − *Department of Chemistry, Southern Methodist University, Dallas, Texas 75275-0314, United States*; ⓞ orcid.org/0000-0002-9658-5626; Email: ekraka@gmail.com

Authors

    Wenli Zou − *Institute of Modern Physics, Northwest University, and Shaanxi Key Laboratory for Theoretical Physics Frontiers, Xi'an, Shaanxi 710127, P. R. China*; ⓞ orcid.org/0000-0002-0747-2428

    Geng-Geng Luo − *Key Laboratory of Environmental Friendly Function Materials, Ministry of Education, and College of Materials Science and Engineering, Huaqiao University, Xiamen, Fujian 361021, P. R. China*

Complete contact information is available at:
https://pubs.acs.org/10.1021/acs.inorgchem.1c03118

Notes

The authors declare no competing financial interest.

ACKNOWLEDGMENTS

REFERENCES

(1) Moss, G. P. Basic Terminology of Stereochemistry (IUPAC Recommendations 1996). *Pure Appl. Chem.* **1996**, *68*, 2193−2222. polytopal rearrangement on page 2213; pseudorotation on page 2215.

(2) Muetterties, E. L. Topological Representation of Stereoisomerism. I. Polytopal Rearrangements. *J. Am. Chem. Soc.* **1969**, *91*, 1636−1643.

(3) Schilter, D. Trading places. *Nat. Rev. Chem.* **2020**, *4*, 2.

(4) Portius, P.; Bühl, M.; George, M. W.; Grevels, F.-W.; Turner, J. J. Structure and Dynamics of Iron Pentacarbonyl. *Organometallics* **2019**, *38*, 4288−4297.

(5) Berry, R. S. Correlation of Rates of Intramolecular Tunneling Processes, with Application to Some Group V Compounds. *J. Chem. Phys.* **1960**, *32*, 933−938.

(6) Berry, R. S. Time-Dependent Measurements and Molecular Structure: Ozone. *Rev. Mod. Phys.* **1960**, *32*, 447−454.

(7) Taha, A. N.; True, N. S.; LeMaster, C. B.; LeMaster, C. L.; Neugebauer-Crawford, S. M. Gas-Phase Nuclear Magnetic Resonance Study of Berry Pseudorotation of SF_4. Comparison of Experimental and Calculated Kinetic Parameters and Falloff Kinetics. *J. Phys. Chem. A* **2000**, *104*, 3341−3348.

(8) Minyaev, R. M.; Wales, D. J. Transition Vector Symmetry and the Internal Pseudo-Rotation and Inversion Paths of ClF_4^+. *J. Chem. Soc., Faraday Trans.* **1994**, *90*, 1831−1837.

(9) Muetterties, E. L. Topological Representation of Stereoisomerism. II. The Five-Atom Family. *J. Am. Chem. Soc.* **1969**, *91*, 4115−4122.
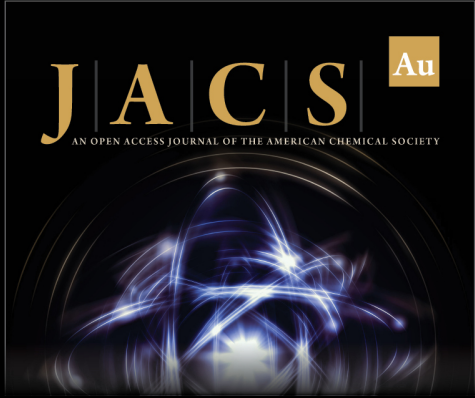
(10) Rzepa, H. S.; Cass, M. E. A Computational Study of the Nondissociative Mechanisms that Interchange Apical and Equatorial Atoms in Square Pyramidal Molecules. *Inorg. Chem.* **2006**, *45*, 3958–3963.

(11) Bailar, J. C., Jr Some Problems in the Stereochemistry of Coordination Compounds: Introductory Lecture. *J. Inorg. Nucl. Chem.* **1958**, *8*, 165–175.

(12) Ray, P.; Dutt, N. Kinetics and Mechanism of Racemization of Optically Active Cobaltic Trisbiguanide Complex. *J. Indian Chem. Soc.* **1943**, *20*, 81–92.

(13) Adams, W. J.; Thompson, H. B.; Bartell, L. S. Structure, Pseudorotation, and Vibrational Mode Coupling in IF_7: An Electron Diffraction Study. *J. Chem. Phys.* **1970**, *53*, 4040–4046.

(14) Lai, J.-C.; Jia, X.-Y.; Wang, D.-P.; Deng, Y.-B.; Zheng, P.; Li, C.-H.; Zuo, J.-L.; Bao, Z. Thermodynamically Stable Whilst Kinetically Labile Coordination Bonds Lead to Strong and Tough Self-Healing Polymers. *Nat. Commun.* **2019**, *10*, 1164 DOI: 10.1038/s41467-019-09130-z.

(15) Flook, M. M.; Börner, J.; Kilyanek, S. M.; Gerber, L. C. H.; Schrock, R. R. Five-Coordinate Rearrangements of Metallacyclobutane Intermediates during Ring-Opening Metathesis Polymerization of 2,3-Dicarboalkoxynorbornenes by Molybdenum and Tungsten Monoalkoxide Pyrrolide Initiators. *Organometallics* **2012**, *31*, 6231–6243.

(16) Khan, R. K. M.; Zhugralin, A. R.; Torker, S.; O'Brien, R. V.; Lombardi, P. J.; Hoveyda, A. H. Synthesis, Isolation, Characterization, and Reactivity of High-Energy Stereogenic-at-Ru Carbenes: Stereochemical Inversion through Olefin Metathesis and Other Pathways. *J. Am. Chem. Soc.* **2012**, *134*, 12438–12441.

(17) Torker, S.; Khan, R. K. M.; Hoveyda, A. H. The Influence of Anionic Ligands on Stereoisomerism of Ru Carbenes and Their Importance to Efficiency and Selectivity of Catalytic Olefin Metathesis Reactions. *J. Am. Chem. Soc.* **2014**, *136*, 3439–3455.

(18) Mikus, M. S.; Torker, S.; Hoveyda, A. H. Controllable ROMP Tacticity by Harnessing the Fluxionality of Stereogenic-at-Ruthenium Complexes. *Angew. Chem., Int. Ed.* **2016**, *55*, 4997–5002.

(19) Rosebrugh, L. E.; Ahmed, T. S.; Marx, V. M.; Hartung, J.; Liu, P.; López, J. G.; Houk, K. N.; Grubbs, R. H. Probing Stereoselectivity in Ring-Opening Metathesis Polymerization Mediated by Cyclometalated Ruthenium-Based Catalysts: A Combined Experimental and Computational Study. *J. Am. Chem. Soc.* **2016**, *138*, 1394–1405.

(20) Dyduch, K.; Roznowska, A.; Srebro-Hooper, M.; Lee, B. Y.; Michalak, A. Theoretical Study on Epoxide Ring-opening in CO2/Epoxide Copolymerization Catalyzed by Bifunctional Salen-Type Cobalt(III) Complexes: Influence of Stereoelectronic Factors. *Catalysts* **2021**, *11*, 328.

(21) Bryant, R. G. The NMR Time Scale. *J. Chem. Educ.* **1983**, *60*, 933.

(22) Chierotti, M. R.; Gobetto, R. Solid-State NMR Investigation of Ligand Mobility and Reactivity in Transition Metal Complexes. *Eur. J. Inorg. Chem.* **2009**, *2009*, 2581–2597.

(23) Nikitin, K.; O'Gara, R. Mechanisms and Beyond: Elucidation of Fluxional Dynamics by Exchange NMR Spectroscopy. *Chem. - Eur. J.* **2019**, *25*, 4551–4589.

(24) Casanova, D.; Cirera, J.; Llunell, M.; Alemany, P.; Avnir, D.; Alvarez, S. Minimal Distortion Pathways in Polyhedral Rearrangements. *J. Am. Chem. Soc.* **2004**, *126*, 1755–1763.

(25) Alvarez, S.; Alemany, P.; Casanova, D.; Cirera, J.; Llunell, M.; Avnir, D. Shape Maps and Polyhedral Interconversion Paths in Transition Metal Chemistry. *Coord. Chem. Rev.* **2005**, *249*, 1693–1708.

(26) Cass, M. E.; Hii, K. K.; Rzepa, H. S. Mechanisms That Interchange Axial and Equatorial Atoms in Fluxional Processes: Illustration of the Berry Pseudorotation, the Turnstile, and the Lever Mechanisms via Animation of Transition State Normal Vibrational Modes. *J. Chem. Educ.* **2006**, *83*, 336.

(27) Rzepa, H. S.; Cass, M. E. In Search of the Bailar and Rây-Dutt Twist Mechanisms That Racemize Chiral Trischelates: A Computational Study of Sc^{III}, Ti^{IV}, Co^{III}, Zn^{II}, Ga^{III}, and Ge^{IV} Complexes of a

Ligand Analogue of Acetylacetonate. *Inorg. Chem.* **2007**, *46*, 8024–8031.

(28) Couzijn, E. P. A.; Slootweg, J. C.; Ehlers, A. W.; Lammertsma, K. Stereomutation of Pentavalent Compounds: Validating the Berry Pseudorotation, Redressing Ugi's Turnstile Rotation, and Revealing the Two- and Three-Arm Turnstiles. *J. Am. Chem. Soc.* **2010**, *132*, 18127–18140.

(29) Asatryan, R.; Ruckenstein, E.; Hachmann, J. Revisiting the Polytopal Rearrangements in Penta-Coordinate d^7-Metallocomplexes: Modified Berry Pseudorotation, Octahedral Switch, and Butterfly Isomerization. *Chem. Sci.* **2017**, *8*, 5512–5525.

(30) Zou, W.; Tao, Y.; Cremer, D.; Kraka, E. Describing Polytopal Rearrangements of Fluxional Molecules with Curvilinear Coordinates Derived from Normal Vibrational Modes: A Conceptual Extension of Cremer-Pople Puckering Coordinates. *J. Chem. Theory Comput.* **2020**, *16*, 3162–3192.

(31) Tao, Y.; Zou, W.; Luo, G.-G.; Kraka, E. Describing Polytopal Rearrangement Processes of Octacoordinate Structures. I. Renewed Insights into Fluxionality of the Rhenium Polyhydride Complex $ReH_5(PPh_3)_2$(Pyridine). *Inorg. Chem.* **2021**, *60*, 2492–2502.

(32) King, R. Structure and Bonding in Homoleptic Transition Metal Hydride Anions. *Coord. Chem. Rev.* **2000**, *200–202*, 813–829.

(33) Mullica, D.; Lok, C.; Grossie, D. A. A New Nine-Coordination System: Pentagonal Interpenetrating Tetrahedral Polyhedron. *J. Solid State Chem.* **1986**, *63*, 452–454.

(34) Ruiz-Martínez, A.; Casanova, D.; Alvarez, S. Polyhedral Structures with an Odd Number of Vertices: Nine-Coordinate Metal Compounds. *Chem. - Eur. J.* **2008**, *14*, 1291–1303.

(35) Knox, K.; Ginsberg, A. P. X-Ray Determination of the Crystal Structure of Potassium Rhenium Hydride. *Inorg. Chem.* **1964**, *3*, 555–558.

(36) Abrahams, S. C.; Ginsberg, A. P.; Knox, K. Transition Metal-Hydrogen Compounds. II. The Crystal and Molecular Structure of Potassium Rhenium Hydride, K_2ReH_9. *Inorg. Chem.* **1964**, *3*, 558–567.

(37) Bronger, W.; à Brassard, L.; Müller, P.; Lebech, B.; Schultz, T. K_2ReH_9, eine Neubestimmung der Struktur. *Z. Anorg. Allg. Chem.* **1999**, *625*, 1143–1146.

(38) Ginsberg, A. P.; Miller, J. M.; Koubek, E. Transition Metal-Hydrogen Compounds. I. Dipotassium Octahydridorhenate(VI). *J. Am. Chem. Soc.* **1961**, *83*, 4909–4915.

(39) Ginsberg, A. P.; Sprinkle, C. R. Transition Metal-Hydrogen Compounds. IV. Improved Synthesis of Enneahydridorhenates: the Sodium and Tetraethylammonium Salts of ReH_9^{2-}. *Inorg. Chem.* **1969**, *8*, 2212–2214.

(40) White, J. W.; Wright, C. J. Internal Vibrations and Hindered Rotation of ReH_9^{-2} by neutron scattering spectroscopy. *J. Chem. Soc., Faraday Trans. 2* **1972**, *68*, 1414–1422.

(41) Creighton, J. A.; Sinclair, T. J. Vibrational Spectrum of the ReH_9^{-2} Ion. *J. Chem. Soc., Faraday Trans. 2* **1974**, *70*, 548.

(42) Parker, S. F.; Refson, K.; Williams, K. P. J.; Braden, D. A.; Hudson, B. S.; Yvon, K. Spectroscopic and Ab Initio Characterization of the $[ReH_9]^{2-}$Ion. *Inorg. Chem.* **2006**, *45*, 10951–10957.

(43) Markopoulos, G.; Kroll, P.; Hoffmann, R. Compressing the Most Hydrogen-Rich Inorganic Ion. *J. Am. Chem. Soc.* **2010**, *132*, 748–755.

(44) Vinitsky, E. A.; Muramatsu, T.; Somayazulu, M.; Wanene, W. K.; Liu, Z.; Chandra, D.; Hemley, R. J. Structural, Vibrational, and Electronic Properties of $BaReH_9$ under Pressure. *J. Phys.: Condens. Matter* **2016**, *28*, 505701.

(45) Shen, M.; Schaefer, H. F.; Partridge, H. The Remarkable Enneahydridorhenate Dianion: ReH_9^{-9}. *Mol. Phys.* **1992**, *76*, 995–1007.

(46) Orgaz, E.; Gupta, M. Electronic structure of $BaReH_9$. *J. Alloys Compd.* **1999**, *293–295*, 217–221.

(47) Li, C.; Agarwal, J.; Schaefer, H. F. The Remarkable $[ReH_9]^{2-}$ Dianion: Molecular Structure and Vibrational Frequencies. *J. Phys. Chem. B* **2014**, *118*, 6482–6490.

(48) Farrar, T. C.; Tsang, T.; Johannesen, R. B. Internal Reorientations in K_2ReH_9 via Wide-Line and Pulsed Proton Resonance Studies. *J. Chem. Phys.* **1969**, *51*, 3595−3596.

(49) Takagi, S.; Ikeshoji, T.; Sato, T.; Orimo, S.-i. Pseudorotating Hydride Complexes with High Hydrogen Coordination: A Class of Rotatable Polyanions in Solid Matter. *Appl. Phys. Lett.* **2020**, *116*, 173901.

(50) Asaji, T. Molecular Motion of Azetidinium Ion and Phase Transition in $[(CH_2)_3NH_2]_2KCo(CN)_6$ with Double Perovskite Structure. *Bull. Chem. Soc. Jpn.* **2021**, *94*, 1659−1663.

(51) Perego, J.; Bracco, S.; Negroni, M.; Bezuidenhout, C. X.; Prando, G.; Carretta, P.; Comotti, A.; Sozzani, P. Fast Motion of Molecular Rotors in Metal-Organic Framework Struts at Very Low Temperatures. *Nat. Chem.* **2020**, *12*, 845−851.

(52) Gonzalez-Nelson, A.; Coudert, F.-X.; van der Veen, M. Rotational Dynamics of Linkers in Metal-Organic Frameworks. *Nanomaterials* **2019**, *9*, 330.

(53) Comotti, A.; Bracco, S.; Ben, T.; Qiu, S.; Sozzani, P. Molecular Rotors in Porous Organic Frameworks. *Angew. Chem., Int. Ed.* **2014**, *53*, 1043−1047.

(54) Wang, X. *Internal Rotation in Molecular Crystals: Computational Studies*; Nova Publishers: New York, 2015.

(55) Heyes, S. J.; Green, M. L. H.; Dobson, C. M. Carbon-13 and Phosphorus-31 CP/MAS NMR Studies of the Polytopal Ligand Rearrangement Process of Tungsten Tris(trimethylphosphine) Hexahydride in the Solid State. *Inorg. Chem.* **1991**, *30*, 1930−1937.

(56) Udovenko, A. A.; Slobodyuk, A. B.; Emelina, T. B.; Laptash, N. M. Fluxional Seven-Coordinated Fluorido- and Oxofluoridotantalates. *Acta Crystallogr., Sect. B: Struct. Sci., Cryst. Eng. Mater.* **2019**, *75*, 1115−1125.

(57) Zhao, Y.; Truhlar, D. G. A New Local Density Functional for Main-Group Thermochemistry, Transition Metal Bonding, Thermochemical Kinetics, and Noncovalent Interactions. *J. Chem. Phys.* **2006**, *125*, 194101.

(58) Weigend, F.; Ahlrichs, R. Balanced Basis Sets of Split Valence, Triple Zeta Valence and Quadruple Zeta Valence Quality for H to Rn: Design and Assessment of Accuracy. *Phys. Chem. Chem. Phys.* **2005**, *7*, 3297.

(59) Weigend, F. Accurate Coulomb-Fitting Basis Sets for H to Rn. *Phys. Chem. Chem. Phys.* **2006**, *8*, 1057.

(60) Neese, F. Software Update: The ORCA Program System, Version 4.0. *WIREs Comput. Mol. Sci.* **2018**, *8*, e1327.

(61) Berendsen, H. J. C.; Postma, J. P. M.; van Gunsteren, W. F.; DiNola, A.; Haak, J. R. Molecular Dynamics with Coupling to An External Bath. *J. Chem. Phys.* **1984**, *81*, 3684−3690.

(62) Frisch, M. J.; Trucks, G. W.; Schlegel, H. B.; Scuseria, G. E.; Robb, M. A.; Cheeseman, J. R.; Scalmani, G.; Barone, V.; Petersson, G. A.; Nakatsuji, H.; Li, X.; Caricato, M.; Marenich, A. V.; Bloino, J.; Janesko, B. G.; Gomperts, R.; Mennucci, B.; Hratchian, H. P.; Ortiz, J. V.; Izmaylov, A. F.; Sonnenberg, J. L.; Williams- Young, D.; Ding, F.; Lipparini, F.; Egidi, F.; Goings, J.; Peng, B.; Petrone, A.; Henderson, T.; Ranasinghe, D.; Zakrzewski, V. G.; Gao, J.; Rega, N.; Zheng, G.; Liang, W.; Hada, M.; Ehara, M.; Toyota, K.; Fukuda, R.; Hasegawa, J.; Ishida, M.; Nakajima, T.; Honda, Y.; Kitao, O.; Nakai, H.; Vreven, T.; Throssell, K.; Montgomery, J. A., Jr.; Peralta, J. E.; Ogliaro, F.; Bearpark, M. J.; Heyd, J. J.; Brothers, E. N.; Kudin, K. N.; Staroverov, V. N.; Keith, T. A.; Kobayashi, R.; Normand, J.; Raghavachari, K.; Rendell, A. P.; Burant, J. C.; Iyengar, S. S.; Tomasi, J.; Cossi, M.; Millam, J. M.; Klene, M.; Adamo, C.; Cammi, R.; Ochterski, J. W.; Martin, R. L.; Morokuma, K.; Farkas, O.; Foresman, J. B.; Fox, D. J. *Gaussian 16*, Revision B.01; Gaussian Inc.: Wallingford CT, 2016.

(63) Liakos, D. G.; Guo, Y.; Neese, F. Comprehensive Benchmark Results for the Domain Based Local Pair Natural Orbital Coupled Cluster Method (DLPNO-CCSD(T)) for Closed- and Open-Shell Systems. *J. Phys. Chem. A* **2020**, *124*, 90−100.

(64) Kresse, G.; Hafner, J. Ab Initio Molecular Dynamics for Liquid Metals. *Phys. Rev. B: Condens. Matter Mater. Phys.* **1993**, *47*, 558−561.

(65) Kresse, G.; Hafner, J. Ab Initio Molecular-Dynamics Simulation of the Liquid-Metal-Amorphous-Semiconductor Transition in Ger-

manium. *Phys. Rev. B: Condens. Matter Mater. Phys.* **1994**, *49*, 14251−14269.

(66) Kresse, G.; Furthmüller, J. Efficiency of Ab-Initio Total Energy Calculations For Metals and Semiconductors Using A Plane-Wave Basis Set. *Comput. Mater. Sci.* **1996**, *6*, 15−50.

(67) Kresse, G.; Furthmüller, J. Efficient Iterative Schemes for Ab Initio Total-Energy Calculations Using A Plane-Wave Basis Set. *Phys. Rev. B: Condens. Matter Mater. Phys.* **1996**, *54*, 11169−11186.

(68) Perdew, J. P.; Burke, K.; Ernzerhof, M. Generalized Gradient Approximation Made Simple. *Phys. Rev. Lett.* **1996**, *77*, 3865−3868.

(69) Perdew, J. P.; Burke, K.; Ernzerhof, M. Erratum: Generalized Gradient Approximation Made Simple [Phys. Rev. Lett. 77, 3865 (1996)]. *Phys. Rev. Lett.* **1997**, *78*, 1396−1396.

(70) Blöchl, P. E. Projector Augmented-Wave Method. *Phys. Rev. B: Condens. Matter Mater. Phys.* **1994**, *50*, 17953−17979.

(71) Kresse, G.; Joubert, D. From Ultrasoft Pseudopotentials to the Projector Augmented-Wave Method. *Phys. Rev. B: Condens. Matter Mater. Phys.* **1999**, *59*, 1758−1775.

(72) Zhang, Y.; Yang, W. Comment on "Generalized Gradient Approximation Made Simple. *Phys. Rev. Lett.* **1998**, *80*, 890−890.

(73) Henkelman, G.; Uberuaga, B. P.; Jónsson, H. A Climbing Image Nudged Elastic Band Method for Finding Saddle Points and Minimum Energy Paths. *J. Chem. Phys.* **2000**, *113*, 9901−9904.

(74) Henkelman, G.; Jónsson, H. Improved Tangent Estimate in the Nudged Elastic Band Method for Finding Minimum Energy Paths and Saddle Points. *J. Chem. Phys.* **2000**, *113*, 9978−9985.

(75) Sheppard, D.; Terrell, R.; Henkelman, G. Optimization Methods for Finding Minimum Energy Paths. *J. Chem. Phys.* **2008**, *128*, 134106.

(76) Baroni, S.; de Gironcoli, S.; Dal Corso, A.; Giannozzi, P. Phonons and Related Crystal Properties from Density-Functional Perturbation Theory. *Rev. Mod. Phys.* **2001**, *73*, 515−562.

(77) Togo, A.; Tanaka, I. First Principles Phonon Calculations in Materials Science. *Scr. Mater.* **2015**, *108*, 1−5.

(78) Streisel, D. J.; Petrou, A. L.; Scorzelli, A. G.; Macalush, B. E.; Siebert, H. M.; Torres, G. S.; Joswick, C. M.; Moehring, G. A. Fluxionality, Substitution, and Hydrogen Exchange at Eight-Coordinate Rhenium(V) Polyhydride Centers. *Inorg. Chim. Acta* **2019**, *496*, 119028.

(79) Guggenberger, L. J.; Muetterties, E. L. Reaction Path Analysis. 2. The Nine-Atom Family. *J. Am. Chem. Soc.* **1976**, *98*, 7221−7225.

(80) Lee, J. C.; Yao, W.; Crabtree, R. H.; Rüegger, H. Fluxionality in $[ReH_5(PPh_3)_2(pyridine)]$. *Inorg. Chem.* **1996**, *35*, 695−699.

(81) Perdew, J. P.; Chevary, J. A.; Vosko, S. H.; Jackson, K. A.; Pederson, M. R.; Singh, D. J.; Fiolhais, C. Atoms, Molecules, Solids, and Surfaces: Applications of the Generalized Gradient Approximation for Exchange and Correlation. *Phys. Rev. B: Condens. Matter Mater. Phys.* **1992**, *46*, 6671−6687.

(82) Perdew, J. P.; Chevary, J. A.; Vosko, S. H.; Jackson, K. A.; Pederson, M. R.; Singh, D. J.; Fiolhais, C. Erratum: Atoms, Molecules, Solids, and Surfaces: Applications of the Generalized Gradient Approximation for Exchange and Correlation. *Phys. Rev. B: Condens. Matter Mater. Phys.* **1993**, *48*, 4978−4978.

(83) Csonka, G. I.; Perdew, J. P.; Ruzsinszky, A.; Philipsen, P. H. T.; Lebègue, S.; Paier, J.; Vydrov, O. A.; Ángyán, J. G. Assessing the Performance of Recent Density Functionals for Bulk Solids. *Phys. Rev. B* **2009**, *79*, 155107 DOI: 10.1103/PhysRevB.79.155107.

(84) Sun, J.; Marsman, M.; Csonka, G. I.; Ruzsinszky, A.; Hao, P.; Kim, Y.-S.; Kresse, G.; Perdew, J. P. Self-Consistent Meta-Generalized Gradient Approximation Within the Projector-Augmented-Wave Method. *Phys. Rev. B* **2011**, *84*, 35117 DOI: 10.1103/PhysRevB.84.035117.

(85) Woessner, D. E.; Gutowsky, H. S. Spin Exchange and Spin-Lattice Relaxation Induced by Mechanical Rotation of Solids. *J. Chem. Phys.* **1958**, *29*, 804−812.

(86) O'Reilly, D. E.; Tsang, T. Deuteron Magnetic Resonance and Proton Relaxation Times in Ferroelectric Ammonium Sulfate. *J. Chem. Phys.* **1967**, *46*, 1291−1300.

(87) Van Vleck, J. H. The Dipolar Broadening of Magnetic Resonance Lines in Crystals. *Phys. Rev.* **1948**, *74*, 1168−1183.

(88) Andrew, E. R.; Eades, R. G.; Allen, J. F. A Nuclear Magnetic Resonance Investigation of Three Solid Benzenes. *Proc. R. Soc. A* **1953**, *218*, 537−552.

(89) Takagi, S.; Iijima, Y.; Sato, T.; Saitoh, H.; Ikeda, K.; Otomo, T.; Miwa, K.; Ikeshoji, T.; ichi Orimo, S. Formation of Novel Transition Metal Hydride Complexes with Ninefold Hydrogen Coordination. *Sci. Rep.* **2017**, *7*, 44253.